Quantum state preparation by adiabatic evolution with custom gates

Eduardo A. Coello Pérez [1,*] Joey Bonitati [2] Dean Lee [2] Sofia Quaglioni [1] and Kyle A. Wendt [1]

[1]*Lawrence Livermore National Laboratory, Livermore, California 94550, USA*

[2]*Facility for Rare Isotope Beams and Department of Physics and Astronomy, Michigan State University, East Lansing, Michigan 48824, USA*

(Received 29 November 2021; accepted 11 February 2022; published 2 March 2022)

Quantum state preparation by adiabatic evolution is currently rendered ineffective by the long implementation times of the underlying quantum circuits, comparable to the decoherence time of present and near-term quantum devices. These implementation times can be significantly reduced by realizing these circuits with custom gates. Using classical computing, we model the output of a realistic two-qubit processor implementing the adiabatic evolution of a two-spin system by means of custom gates. This modeled output is then compared with the results of quantum simulations solving the same problem on IBM Quantum (IBMQ) systems. When used to emulate the behavior of the IBMQ quantum circuit, our realistic model yields state fidelities ranging from 65% to 85%, similar to the actual performance of a diverse set of IBMQ devices. When we reduced the implementation time by using custom gates, however, the loss of fidelity was reduced by at least a factor of 4, allowing us to accurately extract the energy of the target state. This improvement is enough to render adiabatic evolution useful for quantum state preparation for small systems or as a preconditioner for other state preparation methods.

DOI: 10.1103/PhysRevA.105.032403

I. INTRODUCTION

Quantum computing holds the key to efficiently solving problems that are intractable on classical computers [1,2]. One such problem is that of simulating the dynamics of large quantum systems. While the resources required to solve this problem on classical computers grow exponentially with the size of the system, N, its solution on a universal quantum computer would require resources that grow only linearly in N, provided the evolution of the system is driven by local interactions [3,4]. Before the simulation of an interesting system even starts, one must prepare the simulator on a state that corresponds to that of the system at the beginning of its evolution, often the ground state of the system's Hamiltonian. One method to prepare a universal quantum computer with arbitrary precision or fidelity is through adiabatic evolution from a state to which the device has easy access. However, the universal quantum computer that evolves exclusively through controlled operations or quantum gates is just an ideal system. Preparation of present noisy intermediate-scale quantum (NISQ) computers by adiabatic evolution remains a challenge as the long implementation times required to achieve large fidelities enable interactions between the device and its environment to significantly deviate the evolution from its path to the target state.

In the digital quantum computing picture, quantum algorithms are typically implemented using a fixed basis of gates on sets of one and two qubits. Any many-qubit quantum algorithm can be implemented to high precision as a finite series of these gates [5–8]; however, the number of elementary gates required to implement complex quantum algorithms, such as adiabatic evolution, becomes prohibitively large. The short coherence times of modern devices therefore impose a harsh limit on the total run time of an algorithm before the resulting output is indistinguishable from noise. By extending that fixed basis of gates with a few custom gates that are "aware" of the details of the underlying quantum hardware and informed by the algorithm being implemented (e.g., details such as the time propagator between pairs of spins in a spin chain), highly optimized algorithms can be enacted. Often gates on physical quantum hardware are built from some analog signal applied to that quantum device (such as microwave pulses on superconducting transmons) and this approach can be thought of as performing a hybrid digital-analog quantum algorithm. Previously, this strategy has been applied successfully to simulate the real-time evolution of a system of neutron spins to sufficient duration and fidelity to extract spectroscopic information [9,10].

Here, we present a noise-resilient approach to the implementation of arbitrary sequences of unitary transformations using custom quantum gates. In particular, we consider an adiabatic evolution algorithm. We study the implementation of the adiabatic evolution through custom two-qubit gates by modeling a two-qubit processor as two capacitively coupled superconducting transmons driven by microwave pulses and solving the Lindblad master equation for its density matrix with classical computing. We will refer to these classical-computing calculations as "emulations" to distinguish them from simulations performed on a physical quantum processor. In addition, we implement the same adiabatic evolution on IBM Quantum (IBMQ) systems in terms of their native basis set of one- and two-qubit gates. We will refer to the results of these runs as "digital" quantum simulations. We show that, when used to emulate a digital quantum simulation with execution times similar to those achieved on IBMQ

*coelloperez1@llnl.gov

systems, our two-qubit processor model yields state fidelities ranging from 65% to 85%, comparable with those reached by the corresponding IBMQ runs. However, by reducing the length of the microwave pulses realizing the custom gates and, consequently, the implementation time of the adiabatic state preparation, our emulations yield a target state with up to 95% fidelity. We further demonstrate that this gain in fidelity allows one to extract the energy of the target state, a significant improvement over the experiments carried out on IBMQ systems.

The paper is structured as follows. In Sec. II we provide a brief review of adiabatic evolution, set up an algorithm evolving a system of two interacting spins, and discuss the two strategies we used to study the implementation of such an algorithm on quantum computers. Results from both strategies are described in Sec. III. Finally, we summarize the results of this work and outline future research venues in Sec. IV.

II. ADIABATIC EVOLUTION

A controllable quantum system can be slowly driven from the readily accessible ground state of an initial Hamiltonian H_0 into the ground state of an arbitrary Hamiltonian H_T (encoding the dynamics of a desired system) by evolution with a time-dependent Hamiltonian

$$H(t) = f(t)H_0 + g(t)H_T, \tag{1}$$

where $f(t)$ and $g(t)$ are interpolation functions such that

$$f(0) = 1 - g(0) = 1 \text{ and } f(T) = 1 - g(T) = 0. \tag{2}$$

This corresponds to imposing the boundary conditions $H(0) = H_0$ and $H(T) = H_T$. More in general, the adiabatic theorem states that a quantum system initially in the kth eigenstate of H_0 will reach a state arbitrarily close to the kth eigenstate of H_T after a long enough evolution time T, provided the kth eigenvalue is continuous throughout the evolution and does not cross other levels [11]. In terms of the parameter $s \equiv t/T$, the time T required to prepare the quantum device with an error bounded from above by

$$\epsilon = ||P(1) - P_k(1)||, \tag{3}$$

with $P(s)$ and $P_k(s)$ being, respectively, the projectors onto the evolved state and the kth eigenstate of H at time s, is of order [12–14]

$$T \sim O(\max_s(||\partial_s H(s)||)/\Delta^2), \tag{4}$$

where $\Delta = \min_s(|\varepsilon_k(s) - \varepsilon_{k\pm1}(s)|)$ is the minimum energy gap involving the kth eigenvalue throughout the evolution.

The quadratic dependence of the total evolution time T on the inverse of the minimum energy gap, $1/\Delta$, represents a challenge for the use of adiabatic evolution as a method for quantum state preparation on current quantum devices, as well as those expected in the near future. Long evolution times resulting from small energy gaps translate into implementation times long enough for these devices to lose coherence due to their interaction with the environment. Nevertheless, one strong motivation for improving the performance of adiabatic evolution is that it can serve as a preconditioner for other eigenstate preparation methods that require significant overlap between the initial state and the eigenstate of interest, such as phase estimation [15] or the rodeo algorithm [16,17]. Even noisy or incomplete adiabatic evolution can provide a large enhancement of the initial state overlap, thereby significantly improving the performance of the quantum state preparation algorithm applied thereafter. For example, improving the initial state overlap probability from 0.1% to 5% would provide a 50-fold improvement in the algorithmic efficiency.

A. Adiabatic evolution of two-spin systems

In the present study we consider the preparation of a two-spin system in the ground state of the Hamiltonian

$$H_T = -\sigma_1^x\sigma_2^x + \sigma_1^y\sigma_2^y + \frac{1}{2}\sigma_1^z\sigma_2^z - \sum_{i=1}^{2}\sigma_i^z, \tag{5}$$

by initializing the system in the ground state of

$$H_0 = \sum_{i=1}^{2}\sigma_i^x, \tag{6}$$

and performing the adiabatic evolution imposed by the time-dependent Hamiltonian of Eq. (1) with interpolation functions

$$f(t) = \cos^2(\pi t/2T), \quad g(t) = 1 - f(t). \tag{7}$$

We note that the ground state of H_0 is a linear combination of the uncoupled two-spin states,

$$|\phi(0)\rangle = \tfrac{1}{2}(|\downarrow\downarrow\rangle - |\downarrow\uparrow\rangle - |\uparrow\downarrow\rangle + |\uparrow\uparrow\rangle). \tag{8}$$

The ground state of H_T,

$$|\phi(T)\rangle = \mathcal{N}[(-1+\sqrt{2})\,|\downarrow\downarrow\rangle + |\uparrow\uparrow\rangle], \tag{9}$$

with $\mathcal{N}$ a normalization constant, has energy $E_T = -2.328$. Similarly, we can introduce the instantaneous ground state $|\phi(t)\rangle$ of $H(t)$ by solving the time-independent Schrödinger equation $H(t)\,|\phi(t)\rangle = E_t\,|\phi(t)\rangle$ at each instant t. The solution of the time-dependent Schrödinger equation $i\frac{d}{dt}\,|\psi(t)\rangle = H(t)\,|\psi(t)\rangle$ will then approximate $|\phi(t)\rangle$ with (instantaneous) fidelity

$$F(t) = |\langle\phi(t)|\psi(t)\rangle|. \tag{10}$$

For a sufficiently long evolution time T, the state of the system at time T will be very close to the ground state of H_T [see Fig. 1(a)]. Even for a relatively short time of $T = 16$, the infidelity $1 - F(T)$ at the end of the evolution is bounded from above by 10^{-3}. In what follows we set $T = 20$. This choice is a good compromise in anticipation of minimizing, as much as possible, the run time (and hence decoherence error) that one would face when implementing this adiabatic evolution on present-day quantum devices.

The adiabatically evolved state can be expressed in terms of the unitary-time evolution operator for a time-dependent Hamiltonian,

$$|\psi(T)\rangle = \mathcal{U}(0,T)\,|\psi(0)\rangle\,. \tag{11}$$

To implement adiabatic evolution on a quantum device we divide the evolution time into n steps and approximate the evolution operator $\mathcal{U}(0,T)$ as the product of n short-time

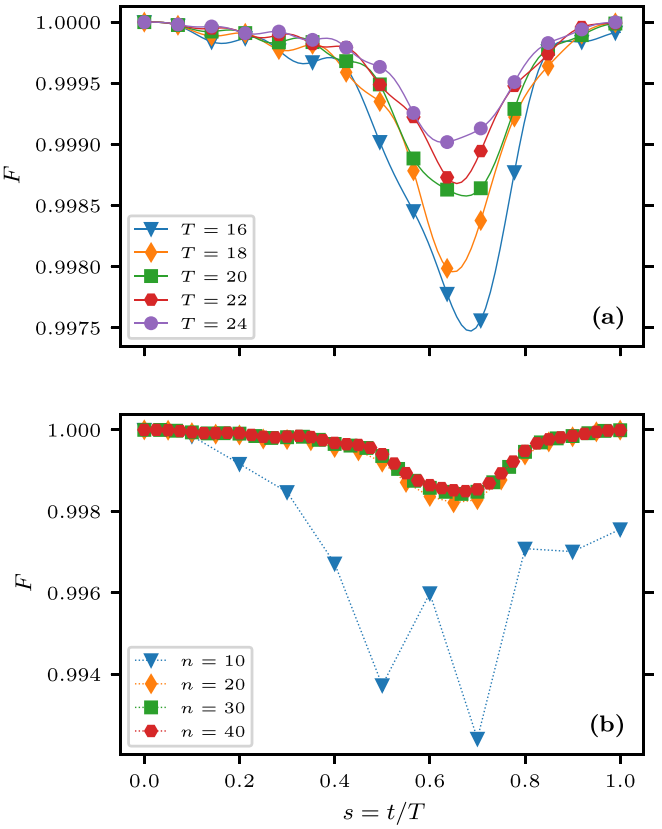

FIG. 1. Evolution of the fidelity between the state of the device and the ground state of $H(t)$ for different values of (a) the evolution time T and (b) the number of time steps n as a function of the parameter $s \equiv t/T$. The adiabatic evolution we implement on quantum devices uses $T = 20$ and $n = 20$, as this combination yields negligible infidelity $1 - F$ at the end of the evolution while minimizing the number of gates required for its implementation.

propagators (for the n instantaneous Hamiltonians)

$$\mathcal{U}(0, T) \approx \prod_{k=1}^{n} U(t_k) = \prod_{k=1}^{n} e^{-iH(t_k)\Delta t}, \tag{12}$$

with $\Delta t = T/n$. The error introduced by the discretization of the evolution time increases with the variation with time of the Hamiltonian, $dH(t)/dt$, and is well behaved provided $H(t_k)$ is a good approximation to the average of $H(t)$ in the time interval $[t_{k-1}, t_k]$ [18]. Thus, the discretization error can be controlled by the number of steps, n, in which the evolution time is divided [see Fig. 1(b), where the fidelity is now evaluated with respect to the solutions $|\psi(t)\rangle$ obtained from the unitary-time evolution of Eq. (11) in the approximation of Eq. (12)]. While larger n values guarantee smaller discretization errors, fewer steps are preferable to minimize the number of quantum gates (circuit depth) required to implement the algorithm on NISQ devices and hence reduce loss of coherence due to interactions with the environment. The results shown in Fig. 1(b) indicate that the discretization error becomes negligible with as few as 20 time steps. Therefore, in what follows we set $n = 20$.

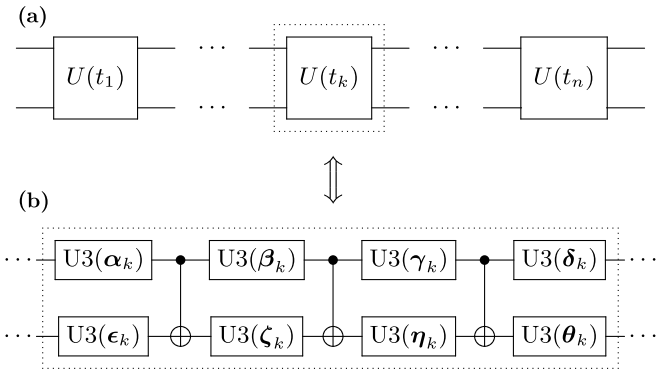

FIG. 2. Decomposition of the kth unitary transformation in the sequence of Eq. (12) [circuit (a)] into CNOT and U3 gates [circuit (b)]. Each U3 gate depends on three Euler angles. The quantum circuit resulting from this decomposition can be directly implemented on IBMQ systems.

B. Implementation on two-qubit devices

Performing a quantum simulation of the adiabatic evolution of Sec. II A requires mapping the spin degrees of freedom to the states of a quantum processor, and translating the short-time propagators $U(t_k)$ in Eq. (12) into quantum gates. The uncoupled states of the two-spin system can be trivially mapped to the computational states of a two-qubit system. Specifically, we use the $|00\rangle$, $|01\rangle$, $|10\rangle$, and $|11\rangle$ states to represent, respectively, the uncoupled two-spin states $|\downarrow\downarrow\rangle$, $|\downarrow\uparrow\rangle$, $|\uparrow\downarrow\rangle$, and $|\uparrow\uparrow\rangle$. Concerning the translation of the short-time propagators into quantum gates, we consider two strategies: (i) a standard decomposition of each propagator into a circuit of elementary gates and (ii) a direct implementation as a single custom two-qubit gate.

The first strategy exploits the fact that any unitary operation involving two qubits, such as the short-time propagators $U(t_k)$ in Eq. (12), can be expressed in terms of three controlled-NOT (CNOT) gates and eight one-qubit U3 gates (constructed from 15 x, y, or z one-qubit rotations) [5–7] as schematically shown in Fig. 2. Such a decomposition can be easily implemented on cloud quantum computing platforms. We studied the performance of this approach by running the adiabatic evolution on several IBMQ systems [19]. The quantum circuit implementing the corresponding algorithm was built using the open-source quantum information software kit (QISKIT) [20], which allowed us to decompose each short-time propagator into elementary gates with the built-in function *quantum_info.two_qubit_cnot_decompose*. The decomposition of the first short-time propagator is explicitly shown in Appendix A as an example. The results of these digital quantum simulations on IBMQ processors are discussed in Sec. III A.

The second strategy employs a realistic model of a physical quantum device to realize each short-time propagator in Eq. (12) with a single custom gate. In the present study, we model a two-qubit processor as two capacitively coupled superconducting transmons controlled by microwave pulses, as schematically shown in Fig. 3(a). The dynamics of this system is described by the Hamiltonian (see Appendix B for

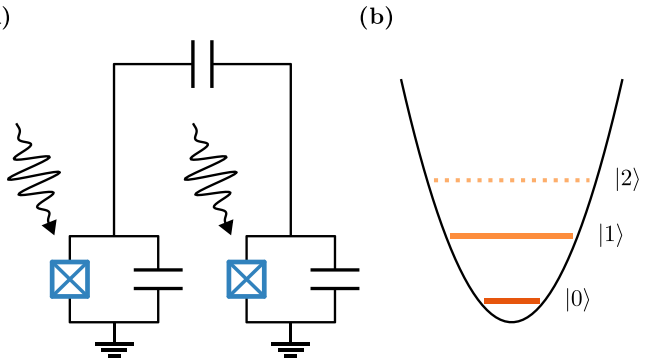

FIG. 3. Schematic representation of (a) the model two-qubit processor, consisting of two capacitively coupled superconducting transmons controlled with microwave pulses, and (b) the energy spectrum of a superconducting transmon in which the lowest two levels, shown as solid lines, are the computational qubit.

details)

$$H_{\mathrm{QPU}}(t) = H_{\mathrm{d}} + H_{\mathrm{c}}(t), \tag{13}$$

where

$$H_{\mathrm{d}} \approx -\sum_{i=1}^{2} \alpha a_i^\dagger a_i a_i^\dagger a_i - g(a_1^\dagger a_2 + a_2^\dagger a_1) \tag{14}$$

is the drift Hamiltonian of the unperturbed device, and

$$H_{\mathrm{c}}(t) = \sum_{i=1}^{2} \left[\epsilon_{\mathrm{I}}^i(t)(a_i^\dagger + a_i) - i\epsilon_{\mathrm{Q}}^i(t)(a_i^\dagger - a_i)\right] \tag{15}$$

is the time-dependent Hamiltonian describing the control of the quantum processor by irradiation with resonant microwave pulses. In the expressions above, $a_i^\dagger$ and a_i are the creation and annihilation operators of transmon i, $\alpha = 200$ MHz is the anharmonicity of both transmons, and $g = 3$ MHz is the strength of the interaction or crosstalk between the transmons due to the capacitive coupling. The time-dependent amplitudes $\epsilon_{\mathrm{I}}^i(t)$ and $\epsilon_{\mathrm{Q}}^i(t)$ are, respectively, the in-phase and quadrature tunable pulse sequences controlling transmon i. In the present study, we take into account the first three energy levels of each transmon. The subspace of states with zero and one quanta per transmon define the computational two-qubit states. The explicit inclusion of states with two quanta in at least one of the transmons provides a description of higher-energy states that can be populated due to gate error and decoherence. It also allows our control pulses to reduce leakage by blocking transitions to these states, as similarly done by the derivative removal by adiabatic gate (DRAG) algorithm [21].

We compute the custom two-qubit gates realizing each of the short-time propagators in Eq. (12) by finding the pulse sequences $\epsilon_{\mathrm{I}}^i(t)$ and $\epsilon_{\mathrm{Q}}^i(t)$ that solve (within an acceptable accuracy) the optimization problem

$$U_{\mathrm{QPU}}(t_k) \simeq \mathcal{U}_{\mathrm{QPU}}(0,\tau) \tag{16}$$
$$= \mathcal{T}\exp\left(-\frac{i}{\hbar}\int_0^\tau [H_{\mathrm{d}} + H_{\mathrm{c}}(\tau')]d\tau'\right),$$

where $U_{\mathrm{QPU}}(t_k)$ represents the short-time propagator $U(t_k)$ embedded into the Hilbert space spanned by the considered two-transmon states and $\mathcal{T}\exp$ denotes the time-ordered exponential. Employing the gradient ascent pulse engineering (GRAPE) algorithm [22], the solution to Eq. (16) is found by minimizing the objective function

$$\Phi = 1 - \frac{F_{\mathrm{gate}}^2}{2} + \chi\frac{\exp(\bar{\epsilon}^{2n}) - 1}{\exp(1) - 1}, \tag{17}$$

where

$$F_{\mathrm{gate}} = \left|\frac{\mathrm{tr}(U_{\mathrm{QPU}}^\dagger \mathcal{U}_{\mathrm{QPU}})}{\dim_{\mathrm{QPU}}}\right|, \tag{18}$$

with $\dim_{\mathrm{QPU}}$ the dimension of the considered Hilbert space, and

$$\bar{\epsilon} = \frac{1}{\epsilon_{\mathrm{cut}}}\sqrt{\frac{1}{\tau}\sum_{i=1}^{2}\sum_{j\in\{\mathrm{I,Q}\}}\int_0^\tau \epsilon_j^i(\tau')^2 d\tau'} \tag{19}$$

the root-mean-squared amplitude of the control pulse normalized to ϵ_{cut}. The gate fidelity F_{gate} in the second term on the right-hand side of Eq. (17) provides an indicator of the accuracy with which the desired unitary operation is reproduced. The last term penalizes large amplitudes through the parameters ϵ_{cut}, which describes the cutoff amplitude, and n, which sets the harshness of the cutoff, all with relevance dictated by the parameter χ. The introduction of this penalty allows one to avoid high-amplitude solutions where the approximation for the Hamiltonian entering the optimization of Eq. (16) is no longer valid, and where hardware realizing the control pulses might not work optimally. The form of this loss term is chosen such that a zero-amplitude pulse yields zero contribution to the total loss and that a pulse the root-mean-square amplitude of which is ϵ_{cut} contributes χ to the total loss. Figure 4 shows the first 100 ns of control pulses realizing the first short-time propagator in the adiabatic evolution algorithm obtained for three different pulse lengths τ of 2500, 400, and 120 ns [see Eq. (16)] and a sampling rate of eight samples per nanosecond. The pulse length $\tau = 2500$ ns was chosen to approximately match the implementation time τ_U of the short-time propagators on the *ibmq_belem* system (see Table I), which will allow us to compare our emulated output to runs on that system. The pulse length $\tau = 400$ is representative of CNOT implementation times on IBMQ systems, while pulses of length $\tau = 120$ ns were the shortest for which the gate infidelity, $1 - F_{\mathrm{gate}}$, could be kept below 10^{-4}. All control pulses were found by minimizing the objective

TABLE I. Calibration data for *ibmq_belem*, *casablanca*, *ibmq_lima*, and *ibmq_manila*. The listed relaxation and dephasing times, T_1 and T_2, are those reported for qubits 0 and 1 of the corresponding system throughout the simulation. Implementation times for the CNOT gate and the decomposition of the short-time propagators are respectively listed as τ_{CNOT} and τ_U.

IBMQ system	T_1 (μs)		T_2 (μs)		τ_{CNOT} (ns)	τ_U (ns)
ibmq_belem	102.6	70.4	127.3	104.5	810.7	≈2500
ibmq_casablanca	111.7	130.1	40.7	102.2	760.9	≈2400
ibmq_lima	101.6	113.0	180.0	106.9	305.8	≈1000
ibmq_manila	136.0	244.2	112.8	46.7	277.3	≈900

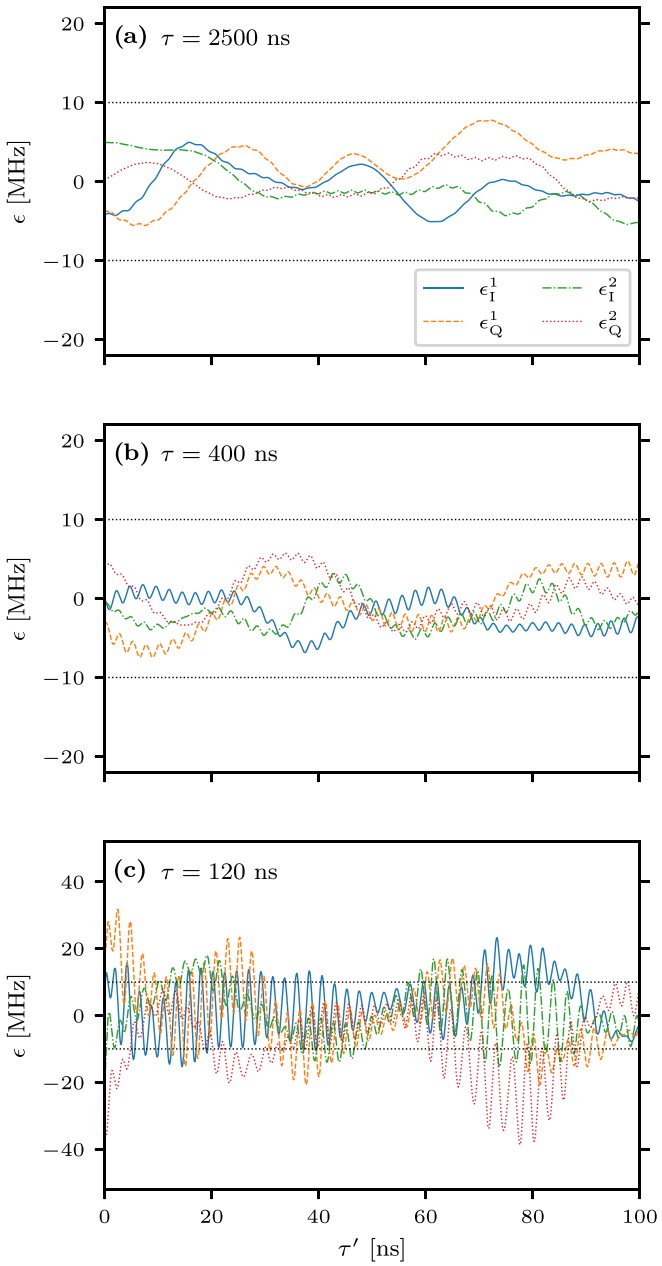

FIG. 4. First 100 ns of the control pulses with lengths (a) $\tau = 2500$ ns, (b) $\tau = 400$ ns, and (c) $\tau = 120$ ns realizing the first unitary in the sequence of Eq. (12). The dependence of the amplitude of the control pulse on its length sets a lower bound for the implementation time of two-qubit gates on present-day quantum devices.

function of Eq. (17) with $\epsilon_{\text{cut}} = 30$ MHz, $n = 3$, and $\chi = 10^{-3}$. Decreasing the length of the control pulse increases the root-mean-squared amplitude as well as the influence of its high-frequency components. This dependence of the amplitude of the control pulse on its length sets a lower bound for the implementation time of two-qubit gates, and hence on the overall implementation time for the whole evolution on present-day quantum devices, as (i) approximations for the Hamiltonian of a quantum computer [used to solve Eq. (16)] and (ii) hardware employed to control it work optimally only within some energy regime.

To study the performance of adiabatic state preparation implemented by means of custom gates obtained through the minimization of Eq. (17), we modeled the output of the two-transmon processor by solving the Lindblad master equations for its density matrix using classical computing. The results of these classical emulations are discussed in Sec. III B.

III. RESULTS

A. Adiabatic evolution of two-spin systems on IBMQ

We perform runs on IBMQ systems to assess how viable it is to implement the adiabatic evolution of Eq. (12) on them using circuits of elementary gates. Relevant calibration data for the used IBMQ systems are listed in Table I. We started each digital quantum simulation by initializing the IBMQ processors in the ground state of the initial Hamiltonian H_0 [see Eq. (6)] by applying the two-qubit Pauli $X^{(2)} = \sigma_1^x \sigma_2^x$ and Hadamard $H^{(2)} = H_1 H_2$ gates to the qubits' lowest state,

$$|\psi(0)\rangle = H^{(2)} X^{(2)} |00\rangle = \tfrac{1}{2}(|00\rangle - |01\rangle - |10\rangle + |11\rangle), \tag{20}$$

and carried out the adiabatic evolution by applying the circuit of elementary quantum gates resulting from the decomposition of the n short-time propagators discussed in Sec. II B.

For each considered IBMQ system, we performed several runs allowing us to approximately reconstruct the evolution of the instantaneous fidelity [see Eq. (10)] and the expectation value of the target Hamiltonian H_T [see Eq. (5)],

$$\langle H_T \rangle(t) = \langle \psi(t) | H_T | \psi(t) \rangle , \tag{21}$$

using quantum expectation estimation (for details see Appendix C). In Fig. 5 we compare the results from runs on IBMQ systems with the emulated output of an ideal quantum processor that does not interact with its environment, obtained with the QISKIT Aer simulator. This ideal output, shown as a dotted line, demonstrates that, for two-qubit systems, gate error does not degrade significantly the fidelity with which the target state is reached. On the other hand, runs on *ibmq_belem*, *ibmq_casablanca*, *ibmq_lima*, and *ibmq_manila*, shown as color markers, deviate from the ideal evolution reaching the target state with fidelities of 60%, 75%, 80%, and 72%, respectively. The loss of fidelity throughout the evolution causes the properties extracted from the reached state to be significantly different from those of the ground state of the target Hamiltonian, as shown by the evolution of $\langle H_T \rangle$ in Fig. 5(b). The energies extracted from runs on IBMQ systems range in mean value from -1.25 to -0.25, whereas the ideal simulation reaches the target value of $E_T = -2.328$. We notice that the rate at which fidelity is lost remains approximately constant throughout the evolution. This is somehow surprising, as our choice for the interpolation functions defining $H(t)$ [see Eq. (7)] is such that the evolution is "slowest" at its beginning and end points (see Fig. 1), where we expected small fidelity losses. The constant rate at which fidelity is lost suggests this effect is dominated by either the gate error accumulated from the elementary gates realizing the short-time propagator (for which the largest contributions come from errors in the CNOT gates) or the loss of coherence along their combined implementation time.

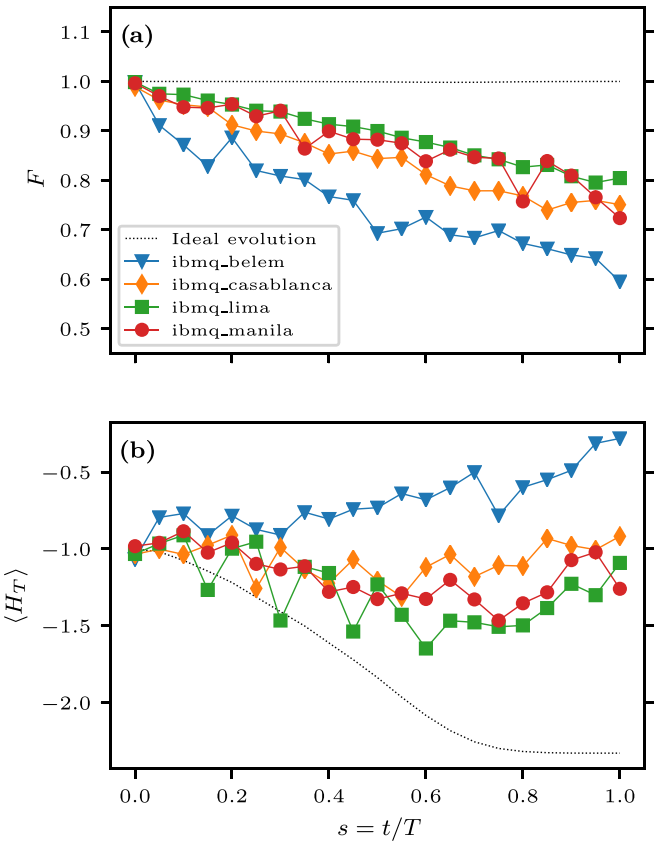

FIG. 5. Evolution of (a) the instantaneous fidelity $F(t)$ and (b) the expectation value $\langle H_T \rangle(t)$ resulting from implementing the sequence of unitaries of Eq. (12) on *ibmq_belem* (blue triangles), *ibmq_casablanca* (orange diamonds), *ibmq_lima* (green squares), and *ibmq_manila* (red circles). Large deviations from simulations on an ideal quantum processor carried out with QISKIT's Aer simulator (dotted lines) result from loss of coherence due to long implementation times.

These results evince the main challenge of quantum state preparation of NISQ devices by means of adiabatic evolution: The implementation time of the quantum circuit expressing the adiabatic evolution of Eq. (12) in terms of elementary gates is comparable to the decoherence times of present quantum devices. Specifically for this work, the implementation times of the adiabatic evolution on *ibmq_belem*, *ibmq_casablanca*, *ibmq_lima*, and *ibmq_manila*, respectively approximated as 52.5, 50.4, 21, and 18.9 μs, are comparable to the relaxation and dephasing decoherence times of these systems, listed as T_1 and T_2 in Table I.

Besides errors due to loss of coherence, simulations on NISQ devices carry measurement errors. These are mitigated in this work by inverting the confusion matrix, extracted from calibration experiments performed at each time step. (For details on the measurement errors and their mitigation see Appendix D.)

B. Classical device-level simulations with customized gates

An alternative to implementing the adiabatic evolution through elementary gates is to find pulse sequences realizing

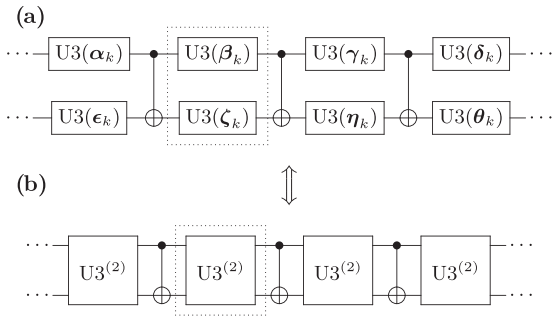

FIG. 6. Combination of simultaneous two U3 gates [circuit (a)] into two-qubit U$^{(2)}$ gates [circuit (b)]. The CNOT and U3$^{(2)}$ gates in circuit (b) are realized with control pulses for which the combined lengths match the implementation time of circuit (a) on IBMQ systems.

the short-time propagators in a single step (see Sec. II B), aiming to reduce the depth of the corresponding circuit and, consequently, its implementation time. To study the performance of this alternative approach, we modeled the output of a two-transmon processor implementing the adiabatic evolution using classical computing (see Sec. II B). Specifically, we used the Quantum Toolbox in PYTHON (QUTIP) [23,24] to solve the Lindblad master equation

$$\begin{aligned}\dot{\rho} = &-\frac{i}{\hbar}[H_{\mathrm{QPU}}, \rho] \\ &+ \frac{1}{T_1}\sum_{i=1}^{2}\left(a_i \rho a_i^\dagger - \frac{1}{2}\{a_i a_i^\dagger, \rho\}\right) \\ &+ \frac{1}{T_2}\sum_{i=1}^{2}\left(a_i^\dagger a_i \rho a_i a_i^\dagger - \frac{1}{2}\{a_i a_i^\dagger a_i^\dagger a_i, \rho\}\right),\end{aligned} \tag{22}$$

for the density ρ of the two-transom system. Here, H_{QPU} is the two-transmon Hamiltonian introduced in Eq. (13) with control pulses optimized to realize the short-time propagators in Eq. (12). The decoherence mechanisms considered by the master equation, relaxation and dephasing, are parametrized by the decoherence times T_1 and T_2, respectively. Our model takes values for these parameters from calibration data of the IBMQ devices on which we implemented the adiabatic evolution (see Table I) to emulate the interaction of these systems with the environment.

First, we emulated the adiabatic evolution in which each of the short-time propagators in Eq. (12) is realized through a single custom gate of pulse length $\tau = 120$ ns. The emulated output reached the target state with fidelities around 95%, greatly improving the results from runs on IBMQ systems, as shown in Figs. 7(a), 7(c), 7(e), and 7(g). While the pulse length $\tau = 120$ ns is the shortest producing gate infidelities below 10^{-4}, the resulting pulse amplitudes surpass the arbitrary threshold $|\epsilon^i_{\mathrm{I,Q}}| < \alpha/20$ (shown as the region between dotted lines in Fig. 4), which could make the corresponding pulses unsuitable for implementation on present-day quantum devices. Next, we emulated the implementation of the algorithm with custom gates of length $\tau = 400$ ns, comparable with the implementation times of the CNOT gate on IBMQ systems. These results still improve over the runs performed

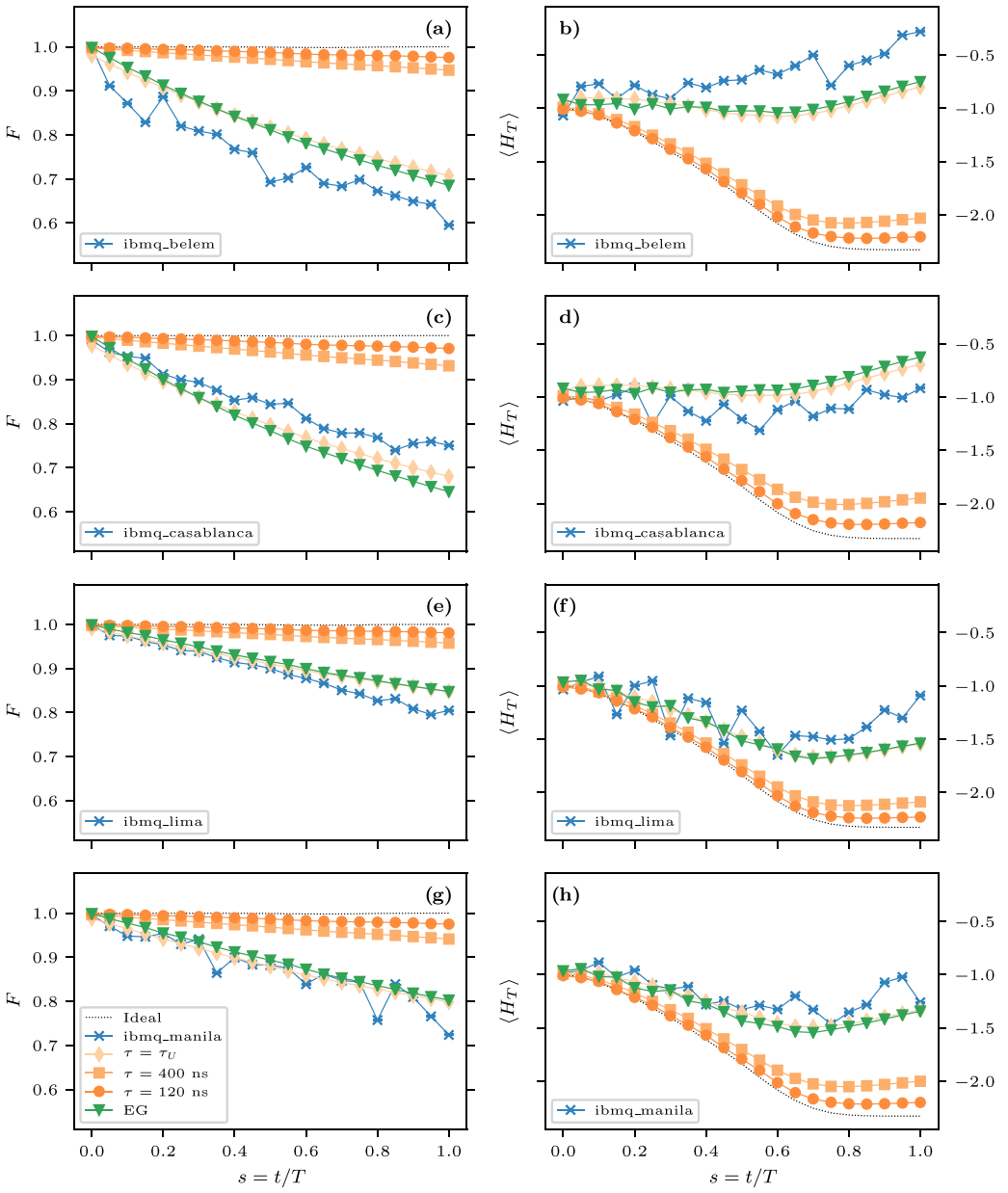

FIG. 7. Comparison between emulated outputs of the adiabatic evolution of Eq. (12) and those from runs on the *ibmq_belem*, *ibmq_casablanca*, *ibmq_lima*, and *ibmq_manila* systems. [(a), (c), (e), (g)] Evolution of the instantaneous fidelity F. Classical emulations implementing the adiabatic evolution through either a circuit of elementary gates or through custom gates of length τ_U (green triangles and orange diamonds, respectively) reach the target state with fidelities comparable to those reached by IBMQ systems (blue crosses). Emulated output using shorter gates (orange squares and circles) reached fidelities around 95%, allowing for a better extraction of the target state's spectroscopic information, as shown by the evolution of $\langle H_T \rangle$ in (b), (d), (f), and (h).

on IBMQ systems, reaching the target state with fidelities around 90%. Finally, to enable a comparison with the IBMQ results, we emulated the adiabatic evolution with custom gates of length approximately matching the implementation time of a short-time propagator on IBMQ systems, τ_U. The values used for τ_U are listed in Table I. The fidelities obtained from these emulations range between 65% and 85%, in good agreement with their IBMQ counterparts. An even more direct comparison can be made by emulating the output of the IBMQ digital quantum simulation itself, i.e., by realizing each elementary gate in the IBMQ quantum circuit with custom control pulses. To conduct these last sets of emulations, we started by combining each pair of simultaneous U3 gates in the short-time propagators into two-qubit $\mathrm{U3}^{(2)} = \mathrm{U3}_1\mathrm{U3}_2$ gates, as schematically shown in Fig. 6. Then, we realized the CNOT and $\mathrm{U3}^{(2)}$ gates with control pulses the combined lengths of which approximately match the implementation time of the short-time propagators on IBMQ systems, τ_U.

In Fig. 7 we compare our emulated outputs to the results of the digital quantum simulations performed on IBMQ systems. The emulated digital quantum simulation (realized by implementing the adiabatic evolution through CNOT and $\mathrm{U3}^{(2)}$

gates), shown as green triangles, closely follows the IBMQ results, shown as blue crosses. The emulated output obtained by realizing the short-time propagators in Eq. (12) in terms of single two-qubit gates with control pulses of lengths $\tau = \tau_U$, $\tau = 400$ ns, and $\tau = 120$ ns, respectively shown as orange diamonds, squares, and circles, make evident the improvement that can be achieved by implementing quantum algorithms through custom gates.

IV. CONCLUSIONS

We presented a noise-resilient approach to the implementation of arbitrary sequences of unitary transformations. In particular, we studied the adiabatic evolution of a two-spin system on NISQ devices. Employing a model of a two-qubit processor consisting of two capacitively coupled superconducting transmons, we emulated the adiabatic evolution implemented with custom two-qubit gates and compared the resulting output with the corresponding results of digital quantum simulations on IBMQ systems. We showed that high-fidelity custom gates for the short-time propagators can be implemented with pulses of varying length, ranging from 2500 to 120 ns, where the lower limit is set by considerations related to the validity of the adopted model and the specifications of standard waveform generators. When the implementation time of the short-time propagators are similar, the state fidelities from our emulated output and IBMQ are comparable, indicating that our two-qubit processor model provides a realistic description of the quantum hardware. As the length of the control pulses realizing the custom gates and, consequently, the implementation time of the adiabatic evolution decreases, the loss of coherence due to the interaction between the quantum computer and its environment is greatly reduced. The fidelities achieved through custom gates greatly improve over those resulting from implementation through elementary gates, reaching the target state with up to 95% fidelity for control pulses with length $\tau = 120$ ns.

High-fidelity quantum state preparation is essential for the subsequent accurate extraction of spectroscopic properties from the desired state. In this study, we demonstrated the extraction of the energy of the state by calculating the expectation value of the target Hamiltonian. The value extracted from our best (i.e., shortest) classical emulation, $\langle H_T \rangle (T) = -2.2$, is in good agreement with the exact result of $E_T = -2.328$. This is a large improvement over the energies extracted from runs on IBMQ systems (ranging in mean value from -1.25 to -0.25) and, more in general, runs on present devices implementing adiabatic evolution through elementary gates. In the future, one can envision obtaining an even higher accuracy by employing the present approach as a preconditioner for other quantum state preparation methods, such as the recently proposed quantum imaginary-time propagation [25] and rodeo algorithms [16].

While in this study we restricted ourselves to the simulation of a simple two-spin system, requiring only two qubits, the use of custom gates can be scaled to more complex simulations involving a larger number of spins by approximating each short-time propagator in terms of propagators for its two-spin subsystems (two-qubit gates). Emulations for such multiparticle systems will require more complex multiqubit processor models with time-varying couplings to minimize unwanted crosstalk among qubits not immediately involved in the propagation. In the future, we plan to explore the adiabatic evolution of linear systems of a larger number of spins. Given the significant advantage of using custom gates demonstrated in this study, it will be also interesting to explore adiabatic evolution on IBMQ using the recently deployed pulse-level access capability. Finally, the significant reduction in implementation time afforded by the proposed use of custom short-time propagator gates opens also the way to noise-resilient simulations of dynamical properties, such as scattering processes, through real-time evolution following preparation with adiabatic evolution.

ACKNOWLEDGMENTS

The authors of this paper would like to thank Jonathan L. DuBois, Yaniv J. Rosen, and Alessandro Roggero for useful discussions. This work was performed under the auspices of the U.S. Department of Energy by Lawrence Livermore National Laboratory under Contract No. DE-AC52-07NA27344. We gratefully acknowledge support from the Laboratory Directed Research and Development (Grant No. 19-DR-005). We also acknowledge financial support from the U.S. Department of Energy (DE-SC0021152 and DE-SC0013365) and the NUCLEI SciDAC-4 collaboration. Computing support for this work came from the LLNL institutional Computing Grand Challenge program. We acknowledge the use of IBMQ services for this work. The views and opinions of authors expressed herein do not necessarily reflect those of IBM or the IBMQ team. In this paper we used *ibmq_belem*, *ibmq_casablanca*, *ibmq_lima* and *ibmq_manila*, some of the IBMQ Falcon Processors.

APPENDIX A: DECOMPOSITION OF A SHORT-TIME PROPAGATOR

As mentioned in Sec. II B, any two-qubit gate can be decomposed into three CNOT gates where the first qubit controls the second one,

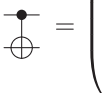

$$= \begin{pmatrix} 1 & 0 & 0 & 0 \\ 0 & 1 & 0 & 0 \\ 0 & 0 & 0 & 1 \\ 0 & 0 & 1 & 0 \end{pmatrix}, \tag{A1}$$

and eight U3 gates, which can be written in terms of x and z one-qubit rotations,

$$\begin{aligned} \mathrm{U3}(\theta, \phi, \lambda) &= R_z(\phi) R_x\left(-\frac{\pi}{2}\right) R_z(\theta) R_x\left(\frac{\pi}{2}\right) R_z(\lambda) \\ &= \begin{pmatrix} \cos\left(\frac{\theta}{2}\right) & -e^{i\lambda} \sin\left(\frac{\theta}{2}\right) \\ e^{i\phi} \sin\left(\frac{\theta}{2}\right) & e^{i(\phi+\lambda)} \cos\left(\frac{\theta}{2}\right) \end{pmatrix}. \end{aligned} \tag{A2}$$

In Fig. 8 we show the quantum circuit resulting from the decomposition in terms of these gates of the first short-time propagator in Eq. (12), obtained using QISKIT's built-in function *quantum_info.two_qubit_cnot_decompose*.

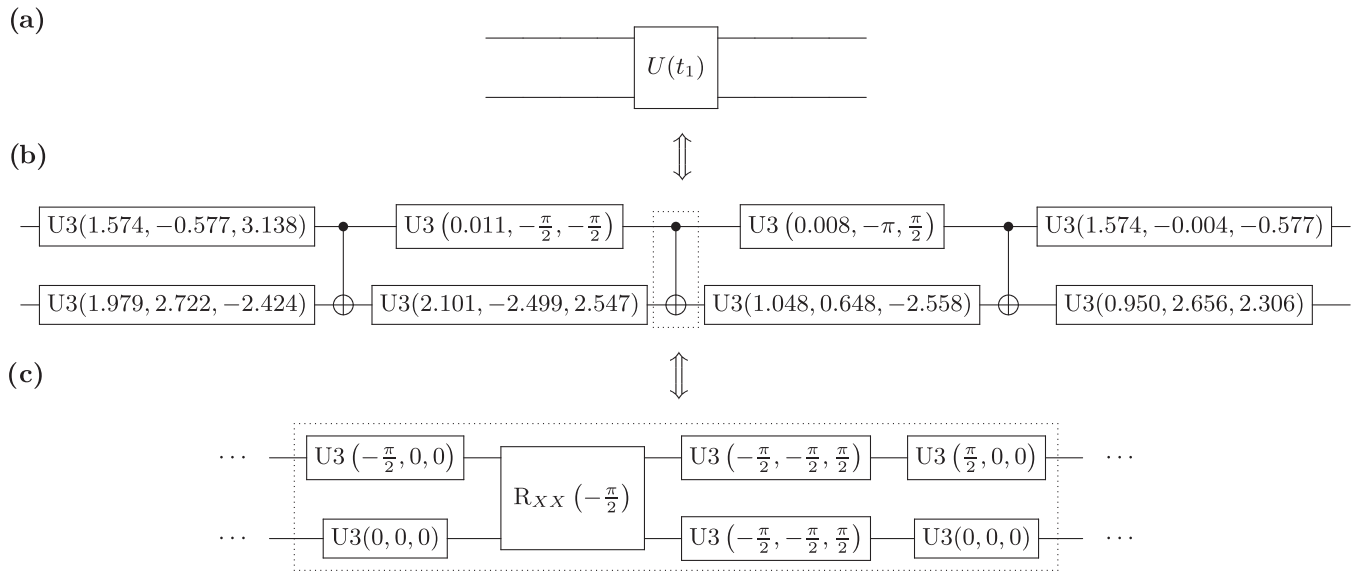

FIG. 8. Decomposition of the first short-time propagator in Eq. (12) [circuit (a)] into CNOT and U3 gates [circuit (b)]. Circuit (c) shows the decomposition of the CNOT gate into elementary gates.

APPENDIX B: MODEL HAMILTONIAN

In terms of the number of Cooper pairs, n, and the flux ϕ, the Hamiltonian of a superconducting transmon up to fourth order in ϕ is [26]

$$\begin{aligned} H &= 4E_C n^2 - E_J \cos(\phi) \\ &\approx 4E_C n^2 - E_J + \frac{E_J}{2}\phi^2 - \frac{E_J}{24}\phi^4, \end{aligned} \tag{B1}$$

where E_C and E_J are respectively the energies stored in the capacitor and Josephson junction. In terms of the transmon's creation and annihilation operators, defined by

$$n = i\left(\frac{E_J}{32E_C}\right)^{\frac{1}{4}}(a^\dagger - a), \quad \phi = \left(\frac{2E_C}{E_J}\right)^{\frac{1}{4}}(a^\dagger + a), \tag{B2}$$

the above Hamiltonian takes the form

$$H \approx \omega a^\dagger a - \frac{\alpha}{6}(a^\dagger + a)^4, \tag{B3}$$

where we defined $\omega \equiv (8E_C E_J)^{1/2}$ and $\alpha \equiv E_C/2$. Using the Baker-Campbell-Hausdorff formula, it can be shown that for a transformation $U = \exp(-i\Omega t a^\dagger a)$

$$U a_1 \cdots a_l U^\dagger = e^{(-i(m-n)\Omega t)} a_1 \cdots a_l, \tag{B4}$$

where $a_1 \cdots a_l$ is a chain of creation and annihilation operators (that is, $a_i \in \{a^\dagger, a\}$), and m and n are the number of creation and annihilation operators in the chain, respectively. Under this transformation, after dropping constant and fast-rotating terms with $|m-n| > 1$, the Hamiltonian of the transmon takes the form

$$\begin{aligned} H \to H' &= UHU^\dagger + i\dot{U}U^\dagger \\ &\approx (\omega + \alpha + \Omega)a^\dagger a - \alpha a^\dagger a a^\dagger a. \end{aligned} \tag{B5}$$

Now, the Hamiltonian of two capacitively coupled transmons controlled by microwave pulses can be approximately written as [27,28]

$$\begin{aligned} H &\approx \sum_{i=1}^{2}\left(4E_{C_i}n_i^2 + \frac{E_{J_i}}{2}\phi_i^2 - \frac{E_{J_i}}{24}\phi_i^4\right) + \frac{8E_{C_1}E_{C_2}}{E_{C_g}}n_1 n_2 \\ &\quad + 2\sum_{i=1}^{2}\eta_i\left[\epsilon_{\mathrm{I}}^i(t)\sin(\Omega_i t) - \epsilon_{\mathrm{Q}}^i(t)\cos(\Omega_i t)\right]n_i \\ &= \sum_{i=1}^{2}\left[\omega_i a_i^\dagger a_i - \frac{\alpha_i}{6}(a_i^\dagger + a_i)^4\right] + g(a_1^\dagger - a_1)(a_2^\dagger - a_2) \\ &\quad + 2i\sum_{i=1}^{2}\left[\epsilon_{\mathrm{I}}^i(t)\sin(\Omega_i t) - \epsilon_{\mathrm{Q}}^i(t)\cos(\Omega_i t)\right](a_i^\dagger - a_i), \end{aligned} \tag{B6}$$

where the term proportional to $g \equiv 8E_{C_1}E_{C_2}/E_{C_g}\eta_1\eta_2$ with $\eta_i \equiv (32E_{C_i}/E_{J_i})^{1/4}$ describes the interaction or crosstalk between the transmons due to its capacitive coupling. Under the transformation

$$U = \exp(-i\Omega_1 t a_1^\dagger a_1 - i\Omega_2 t a_2^\dagger a_2), \tag{B7}$$

with $\Omega_i = -\omega_i - \alpha_i$, the above Hamiltonian takes the form

$$\begin{aligned} H &\approx -\sum_{i=1}^{2}\alpha_i a_i^\dagger a_i a_i^\dagger a_i - g(a_1^\dagger a_2 + a_1 a_2^\dagger) \\ &\quad + \sum_{i=1}^{2}\left[\epsilon_{\mathrm{I}}^i(t)(a_i^\dagger + a_i) - i\epsilon_{\mathrm{Q}}^i(t)(a_i^\dagger - a_i)\right], \end{aligned} \tag{B8}$$

after dropping constant and fast-rotating terms, and assuming that $\Omega_1 \approx \Omega_2$.

APPENDIX C: QUANTUM EXPECTATION ESTIMATION

Quantum computers are generally measured in the eigenbasis of the Pauli Z matrix. Measuring an ensemble of systems

in the state $|\psi\rangle$ yields the occupation probabilities $|c_{q_1 q_2 \cdots q_n}|^2$, where the expansion coefficients $c_{q_1 q_2 \cdots q_n}$ are defined by

$$|\psi\rangle = \sum_{q_1, q_2, \ldots, q_n \in \{0,1\}} c_{q_1 q_2 \cdots q_n} |q_1 q_2 \cdots q_n\rangle . \tag{C1}$$

The expectation value of the two-spin operator $\sigma_1^z \sigma_2^z$ in the two-qubit state $|\psi\rangle$ can be easily extracted from experiments due to the fact that this operator is diagonal in the measurement basis:

$$\begin{aligned} \langle\psi| \sigma_1^z \sigma_2^z |\psi\rangle &= \sum_{i,j,k,l \in \{0,1\}} \langle\psi|ij\rangle \langle ij| \sigma_1^z \sigma_2^z |kl\rangle \langle kl|\psi\rangle \\ &= \sum_{i,j \in \{0,1\}} \langle ij| \sigma_1^z \sigma_2^z |ij\rangle |c_{ij}|^2. \end{aligned} \tag{C2}$$

Now, the expectation value of a general two-spin operator $\sigma_1^a \sigma_2^b$ with $a, b \in \{0, x, y, z\}$ ($\sigma_i^0 \equiv I_i$, the identity operator) in the state $|\psi\rangle$ can also be extracted from experiments by means of any unitary transformation U such that

$$U \sigma_1^a \sigma_2^b U^\dagger = \sigma_1^z \sigma_2^z, \tag{C3}$$

as

$$\begin{aligned} \langle\psi| \sigma_1^a \sigma_2^b |\psi\rangle &= \langle\psi| U^\dagger U \sigma_1^a \sigma_2^b U^\dagger U |\psi\rangle = \langle\psi'| \sigma_1^z \sigma_2^z |\psi'\rangle \\ &= \sum_{i,j \in \{0,1\}} \langle ij| \sigma_1^z \sigma_2^z |ij\rangle |c'_{ij}|^2, \end{aligned} \tag{C4}$$

where

$$|\psi'\rangle = U |\psi\rangle = \sum_{i,j \in \{0,1\}} c'_{ij} |ij\rangle . \tag{C5}$$

Thus, it is possible to extract the expectation value of any Hamiltonian of the form

$$H = \sum_{a,b \in \{0,x,y,z\}} h_{ab} \sigma_1^a \sigma_2^b, \tag{C6}$$

such as the two-spin Hamiltonian of Eq. (5). In this work, we employed the transformations $U_x = u_1^x u_2^x$ and $U_y = u_1^y u_2^y$ with

$$u_i^x = \mathrm{U3}\Big(\frac{\pi}{2}, 0, \pi\Big), \quad u_i^y = \mathrm{U3}\Big(\frac{\pi}{2}, \frac{\pi}{2}, \frac{\pi}{2}\Big), \tag{C7}$$

to extract the expectation values of $\sigma_1^x \sigma_2^x$ and $\sigma_1^y \sigma_2^y$, respectively.

To approximately extract the fidelity at time t_k, $F(t_k)$, we take advantage of the fact that [see Eqs. (12) and (20)]

$$\begin{aligned} \langle\phi(t_k)| \approx \langle\psi(t_k)| &= \langle 00| X^{(2)} H^{(2)} \mathcal{U}^\dagger(0, t_k) \\ &\approx \langle 00| X^{(2)} H^{(2)} \prod_{i=k}^{1} U^\dagger(t_i), \end{aligned} \tag{C8}$$

and decompose the overall unitary operator

$$\widetilde{U}(t_k) = X^{(2)} H^{(2)} \prod_{i=k}^{1} U^\dagger(t_i) \tag{C9}$$

into a single circuit with QISKIT and apply it at the end of the evolution. This yields

$$\begin{aligned} F(t_k) &= |\, \langle\phi(t_k)|\psi(t_k)\rangle \,| \approx |\, \langle 00|\, \widetilde{U}(t_k)\, |\psi(t_k)\rangle \,| \\ &= |\, \langle 00|\widetilde{\psi}(t_k)\rangle \,| \\ &= |\widetilde{c}_{00}|. \end{aligned} \tag{C10}$$

APPENDIX D: MEASUREMENT ERRORS

The measurement error mitigation scheme follows closely that employed and discussed in Ref. [29]. Let the probability to measure a qubit in the state $|i\rangle$ when it was prepared in state $|j\rangle$ be p_{ij}. The occupation probabilities measured in an experiment, arranged in the vector $|c^2_{\mathrm{exp}}\rangle$, are related to the true ones, $|c^2_{\mathrm{true}}\rangle$, through the confusion or error matrix P

$$\big||c|^2_{\mathrm{exp}}\big\rangle = P\,\big||c|^2_{\mathrm{true}}\big\rangle \quad \text{or} \quad \big||c|^2_{\mathrm{true}}\big\rangle = P^{-1}\,\big||c|^2_{\mathrm{exp}}\big\rangle, \tag{D1}$$

constructed from the probabilities to measure a two-qubit system in the state $|ij\rangle$ when it was prepared in the state $|kl\rangle$, denoted by $p_{ij,kl}$. Under the assumption that the measurement errors in qubits 1 and 2 are independent of each other, the confusion matrix can be written in terms of the single-qubit measurement probabilities p_{ij} as

$$P \approx \begin{pmatrix} (1-p_{10})_1(1-p_{10})_2 & (1-p_{10})_1(p_{01})_2 & (p_{01})_1(1-p_{10})_2 & (p_{01})_1(p_{01})_2 \\ (1-p_{10})_1(p_{10})_2 & (1-p_{10})_1(1-p_{01})_2 & (p_{01})_1(p_{10})_2 & (p_{01})_1(1-p_{01})_2 \\ (p_{10})_1(1-p_{10})_2 & (p_{10})_1(p_{01})_2 & (1-p_{01})_1(1-p_{10})_2 & (1-p_{01})_1(p_{01})_2 \\ (p_{10})_1(p_{10})_2 & (p_{10})_1(1-p_{01})_2 & (1-p_{01})_1(p_{10})_2 & (1-p_{01})_1(1-p_{01})_2 \end{pmatrix}. \tag{D2}$$

At the beginning of each time step, we perform two calibration experiments, preparing the device in the states $|00\rangle$ and $|11\rangle$. The measurements of these experiments correspond to the first and fourth columns of the confusion matrix. From them, we can extract the single-qubit measurement probabilities, p_{ij}, and construct the full confusion matrix.

APPENDIX E: IDENTIFICATION OF DOMINANT ERROR SOURCES

There are several sources of error affecting the implementation of adiabatic evolution on IBMQ hardware. Among them, in our model we account for systematic gate infidelities, stochastic dissipative processes during the circuit execution, stochastic measurement error during readout, and statistical noise. The impact of these sources of error on the adiabatic evolution can be studied by contrasting simulations based on QISKIT's Aer simulator, and runs on IBMQ systems. We start running simulations with QISKIT's Aer simulator to measure the state $H^{(2)}|00\rangle = (|00\rangle + |01\rangle + |10\rangle + |11\rangle)/2$, using the *AerSimulator.from_backend* method. This constructs a classical simulator with an approximate noise model for any IBMQ device that includes gate errors, readout errors, and dissipative processes. Figure 9 shows the average deviation of

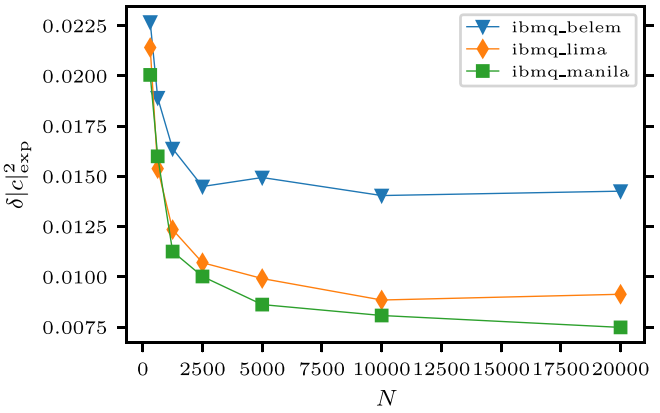

FIG. 9. Average error in measured occupation probabilities with the number of shots, N. Increasing the number of shots decreases the statistical noise yielding an estimate for the quantum computer's measurement error. The error in the occupation probabilities yielded by these simulations are bounded from above by $\delta|c|^2_{\text{exp}} = 0.016$, accounting for only a small fraction of the error observed in calculated fidelities and expectation values.

the measured occupation probabilities from their ideal value, 1/4, with the number of shots, N. As N is increased, the statistical component of the error becomes negligible and the average error reaches a device-dependent plateau, that we identify with the measurement error of each IBMQ system. Results from these simulations suggest that measurement and statistical noise are not dominant sources of error, as they account for deviations from ideal fidelities and expectation values (for IBMQ runs considering $N = 2500$ shots) of approximately $\delta F \approx 0.01$ and $\delta \langle H_T \rangle \approx 0.1$, much smaller from those shown in Fig. 7.

Next, we ran simulations of the adiabatic evolution with QISKIT's Aer simulator choosing the *"statevector"* method and saving per-shot amplitudes (this unfortunately disables the simulation of readout error). We simulate 100 000 shots for each circuit needed to compute the evolving instantaneous fidelity and the instantaneous ground-state energy. Using the stored amplitudes, we compute the energy for each simulated shot following Eq. (C4), yielding the distribution of possible energies, and repeat a similar process for the fidelity. To disentangle the impact of dissipative processes from all other sources of error, we construct the density matrix for each circuit by averaging over the shots:

$$\rho = \frac{1}{N_{\text{shots}}} \sum_{i \in \text{shots}} |i\rangle \langle i| , \tag{E1}$$

where $|i\rangle$ is the final state of the simulated circuits. We then compute the singular value decomposition of the density to find the most likely state, i.e., the state with largest singular value, and compute the fidelity and energy using those amplitudes. In the presence of only gate infidelity and readout errors, there should be one singular value very close to one; however, the dissipative processes will produce mixed states and the largest singular value will be significantly less that

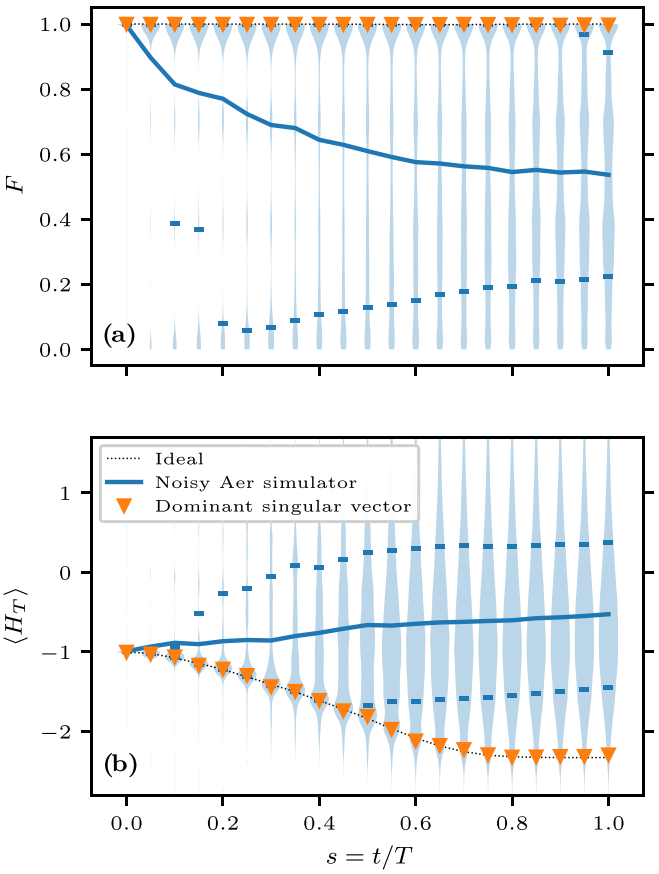

FIG. 10. Evolution of **a)** the fidelity and **b)** expectation value $\langle H_T \rangle$ with Qiskit's Aer simulator and a noise model based on *ibmq_belem*. Solid blue lines show the expect output when including all error sources considered by Aer, while the blue shaded regions indicate the distributions of likely values at each time step. Dotted black lines indicate the ideal evolution that a noiseless device would yield. Orange triangles result from a singular value decomposition filtering of the data underlying the blue distributions. The similarities between dotted lines and orange triangles strongly suggest that dissipative processes are by far the dominant source of noise in IBMQ simulations, even very early in the evolution.

its ideal value, decreasing with the circuit depth. In Fig. 10 we plot the resulting distributions at each step for both the fidelity [Fig. 10(a)] and the expectation value [Fig. 10(b)] of the target Hamiltonian as blue violin plots showing the mean and 1σ quantiles. The green lines show the answer expected from an ideal evolution, while the orange dashed lines show results using the largest singular vector of density matrices. The difference between the dashed orange and solid blue lines results almost entirely from dissipative noise processes, which in contrast to the closeness of the dashed orange and solid green lines indicates again that other errors are extremely minor in comparison. The blue markers give a measure of the lower bound on the total uncertainty that we can anticipate from simulations on IBMQ systems.

[1] M. A. Nielsen and I. L. Chuang, *Quantum Computation and Quantum Information* (Cambridge University Press, Cambridge, U.K., 2010).
[2] A. Steane, Rep. Prog. Phys. **61**, 117 (1998).
[3] S. Lloyd, Science **273**, 1073 (1996).
[4] R. P. Feynman, Int. J. Theor. Phys. **21**, 467 (1982).
[5] V. V. Shende, I. L. Markov, and S. S. Bullock, Phys. Rev. A **69**, 062321 (2004).
[6] F. Vatan and C. Williams, Phys. Rev. A **69**, 032315 (2004).
[7] G. Vidal and C. M. Dawson, Phys. Rev. A **69**, 010301(R) (2004).
[8] A. Barenco, C. H. Bennett, R. Cleve, D. P. DiVincenzo, N. Margolus, P. Shor, T. Sleator, J. A. Smolin, and H. Weinfurter, Phys. Rev. A **52**, 3457 (1995).
[9] X. Wu, K. A. Wendt, E. A. Coello Pérez, K. Kravvaris, L. Martinez, L. Castelli, Y. J. Rosen, W. E. Ormand, F. Pederiva, J. L. DuBois, and S. Quaglioni (unpublished).
[10] E. T. Holland, K. A. Wendt, K. Kravvaris, X. Wu, W. E. Ormand, J. L. DuBois, S. Quaglioni, and F. Pederiva, Phys. Rev. A **101**, 062307 (2020).
[11] M. Born and V. Fock, Z. Phys. **51**, 165 (1928).
[12] T. Albash and D. A. Lidar, Rev. Mod. Phys. **90**, 015002 (2018).
[13] S. Boixo and R. D. Somma, Phys. Rev. A **81**, 032308 (2010).
[14] S. Boixo, E. Knill, and R. D. Somma, Quantum Inf. Comput. **9**, 833 (2009).
[15] A. Yu. Kitaev, arXiv:quant-ph/9511026.
[16] K. Choi, D. Lee, J. Bonitati, Z. Qian, and J. Watkins, Phys. Rev. Lett. **127**, 040505 (2021).
[17] Z. Qian, J. Watkins, G. Given, J. Bonitati, K. Choi, and D. Lee, arXiv:2110.07747.
[18] D. Poulin, A. Qarry, R. Somma, and F. Verstraete, Phys. Rev. Lett. **106**, 170501 (2011).
[19] IBM Quantum (2021), https://quantum-computing.ibm.com.
[20] M. S. Anis *et al.*, QISKIT: An open-source framework for quantum computing (2021).
[21] F. Motzoi, J. M. Gambetta, P. Rebentrost, and F. K. Wilhelm, Phys. Rev. Lett. **103**, 110501 (2009).
[22] N. Khaneja, T. Reiss, C. Kehlet, T. Schulte-Herbrüggen, and S. J. Glaser, J. Magn. Reson. **172**, 296 (2005).
[23] J. R. Johansson, P. D. Nation, and F. Nori, Comput. Phys. Commun. **184**, 1234 (2013).
[24] J. R. Johansson, P. D. Nation, and F. Nori, Comput. Phys. Commun. **183**, 1760 (2012).
[25] F. Turro, V. Amitrano, P. Luchi, A. Roggero, K. A. Wendt, J. L. DuBois, S. Quaglioni, and F. Pederiva, arXiv:2102.12260.
[26] J. Koch, T. M. Yu, J. Gambetta, A. A. Houck, D. I. Schuster, J. Majer, A. Blais, M. H. Devoret, S. M. Girvin, and R. J. Schoelkopf, Phys. Rev. A **76**, 042319 (2007).
[27] T. Jones, K. Steven, X. Poncini, M. Rose, and A. Fedorov, Phys. Rev. Appl. **16**, 054039 (2021).
[28] P. Krantz, M. Kjaergaard, F. Yan, T. P. Orlando, S. Gustavsson, and W. D. Oliver, Appl. Phys. Rev. **6**, 021318 (2019).
[29] A. Roggero, C. Gu, A. Baroni, and T. Papenbrock, Phys. Rev. C **102**, 064624 (2020).